Nuclear Engineering and Design 346 (2019) 209–219

Contents lists available at ScienceDirect

Nuclear Engineering and Design

journal homepage: www.elsevier.com/locate/nucengdes

Development of an SP_3 neutron transport solver for the analysis of the Molten Salt Fast Reactor

E. Cervi, S. Lorenzi, A. Cammi, L. Luzzi*

Politecnico di Milano, Department of Energy, Nuclear Engineering Division, Via La Masa 34, 20156 Milan, Italy

ARTICLE INFO

Keywords:
Multiphysics
OpenFOAM
Neutron transport
Molten Salt Fast Reactor (MSFR)

ABSTRACT

The aim of this paper is the extension of a multiphysics OpenFOAM solver for the analysis of the Molten Salt Fast Reactor (MSFR), developed in previous works (Cervi et al., 2017, 2018). In particular, the neutronics sub-solver is improved by implementing a new module based on the SP_3 approximation of the neutron transport equation. The new module is successfully tested against a Monte Carlo model of the MSFR, in order to assess its correct implementation. Then, a neutronics analysis of the MSFR is carried out on a simplified axial-symmetric model of the reactor. Particular focus is devoted to the analysis of the MSFR helium bubbling system and its effect on reactivity. The presence of bubbles inside the reactor is handled with a two-fluid thermal-hydraulics module, previously implemented into the solver. The void reactivity coefficient is evaluated on the basis of the bubble spatial distribution calculated by the multiphysics solver. Then, the results are compared to simulations carried out with uniform bubble distributions, highlighting significant differences between the two approaches. The outcomes of this work constitute a step forward in the multiphysics analysis of the Molten Salt Fast Reactor and represent a useful starting point for the optimization of the MSFR helium bubbling system, as well as for the development of appropriate control strategies.

1. Introduction

The Molten Salt Fast Reactor (MSFR) developed in the framework of the H2020 SAMOFAR Project (http://samofar.eu/) is a circulating fuel nuclear reactor in which a mixture of molten thorium and uranium fluorides acts as fuel and coolant simultaneously (Gerardin et al., 2017). Thanks to its intrinsic characteristics of safety and sustainability, the MSFR is raising a growing interest in the nuclear reactor community, both from a scientific and industrial viewpoint. Firstly, the adoption of a closed thorium fuel cycle leads to an actinide inventory with lower radiotoxicity. In addition, fast reactors are also of interest for the purpose of breeding fissile isotopes from fertile nuclides, significantly extending the availability of fuel resources (Fiorina et al., 2013). Finally, the high boiling temperature of molten salts allows operation at atmospheric pressure, reducing the mechanical load on structural materials and, as a consequence, greatly improving the safety of the system.

Compared to traditional solid-fuelled reactors, the circulating fuel is a distinguishing feature of the MSFR and other Molten Salt Reactors as well – e.g., see Serp et al. (2014), Dolan (2017) –, which arises completely new design and technological challenges. Notably, the delayed neutron precursors are not static, as in conventional nuclear systems, but they are dragged by the fuel mixture through the reactor and the external circuits. For this reason, delayed neutrons can be emitted in peripheral regions of the reactor, where the neutron importance is lower, or even in the external circuit, where they do not contribute to the fission chain reaction. As a consequence, the coupling between the neutronics and thermo-fluid-dynamics of the system is even stronger than in traditional reactors, since the fuel velocity field directly influences the precursor distribution. In this regard, the multiphysics approach provides a good way to inherently couple all the physical phenomena occurring in the reactor in the same simulation environment, offering a more efficient way to handle the coupling non-linearities (Ragusa and Mahadevan, 2009). Multiphysics models of the MSFR have been developed by Cammi et al. (2011, 2012), Aufiero et al. (2014a,b), Fiorina et al. (2013, 2014), coupling the neutron diffusion equation with a single-phase, incompressible thermal-hydraulics model. Transport equations for the moving precursors are also implemented (Aufiero et al., 2014b). More studies are proposed by Wang et al. (2006), using the SIMMER-III code, and by Hu et al. (2017), based on OpenMC/TANSY.

A helium bubbling system is foreseen in the MSFR for a more efficient removal of gaseous fission products (Delpech et al., 2009). The

* Corresponding author.
E-mail address: lelio.luzzi@polimi.it (L. Luzzi).

https://doi.org/10.1016/j.nucengdes.2019.03.001
Received 10 November 2018; Received in revised form 26 February 2019; Accepted 1 March 2019

Nomenclature

Latin symbols

c	Delayed neutron precursor density, m^{-3}
d	Decay heat precursor density, m^{-3}
K_D	Doppler constant, pcm
Sc	Schmidt number, –
t	Time, s
T	Temperature, K
$\boldsymbol{u}$	Fuel velocity, $m\,s^{-1}$
v_i	Neutron velocity, $m\,s^{-1}$

Greek symbols

$\bar{\alpha}_b$	Core-average void fraction, –
α_i	Albedo coefficient, –
α_l	Liquid phase fraction, –
α_{void}	Void coefficient, pcm/%
β	Delayed neutron fraction, –
λ	Delayed neutron precursor decay constant, s^{-1}
λ_h	Decay heat precursor decay constant, s^{-1}
ν	Kinematic viscosity, $m^2\,s^{-1}$
$\bar{\nu}$	Average neutrons per fission, –
ρ	Density, $kg\,m^{-3}$
ρ	Reactivity, pcm
Σ	Macroscopic cross section, m^{-1}
σ	Standard deviation, –
φ_0	Neutron flux, $m^{-2}\,s^{-1}$
φ_2	Second neutron flux moment, $m^{-2}\,s^{-1}$
χ	Neutron yield, –

Subscripts

d	Delayed
f	Fission
h	Heat
i, j	Neutron energy group
k	Delayed neutron precursor group
m	Decay heat precursor group
p	Prompt
r	Removal
s	Scattering
$s2$	Second order inelastic scattering
$s3$	Third order inelastic scattering
T	Turbulent
t	Total
tr	Transport

helium bubbling is also envisaged as a possible option for the reactivity control of the MSFR, exploiting the void reactivity effect of the gas bubbles. This design choice would replace the control rods, traditionally employed for reactivity control of conventional solid-fuelled reactors. Therefore, careful investigation is needed in order to assess the feasibility and the safety of this option. Furthermore, the liquid fuel compressibility, further increased by the helium bubbles, is expected to have a strong impact on fast, reactivity-driven transients, where the finite propagation velocity of pressure waves can lead to delays in the expansion reactivity feedback. Fast, reactivity-driven transients could be a reason of concern in the start-up phase of the reactor, due to unwanted injection of large fuel quantities, or in case of a sudden failure of the helium bubbling system (Cervi et al., 2019). Both the helium bubbling system and compressibility effects cannot be described by means of standard single-phase, incompressible thermal-hydraulics models. To address these issues, a multiphysics OpenFOAM solver has been developed by Cervi et al. (2019), coupling the multi-group neutron diffusion equation with a two-fluids (or Euler-Euler, see Rusche, 2002) model for two-phase, compressible thermal-hydraulics. As in previous solvers, the motion of precursors in the liquid fuel is also considered. OpenFOAM is a CFD and multiphysics toolkit based on the finite volume method (Moukalled et al., 2016) for the discretization of high-fidelity partial differential equations. Complete documentation can be found on the OpenFOAM website (OpenFOAM, 2013).

While the impact of fuel compressibility in fast transients has been studied by Cervi et al. (2019), few information is currently available on the effect of the helium bubbling system on the MSFR reactivity. To fill this gap, the present work aims at estimating the void reactivity coefficient of the helium bubbles. This analysis focuses in particular on the effect of the bubble spatial distribution, which may affect the value of the void coefficient through spatial and neutron importance effects.

As for the neutronics modelling, neutron diffusion is typically selected for the estimation of the neutron flux in available multiphysics models of the MSFR. However, the adoption of more accurate neutronics models, based on transport theory, may constitute an improvement for the analysis of the MSFR, allowing for catching phenomena that cannot be described by means of diffusion approaches. It is well known that diffusion theory has some limits, especially when it comes to predicting the neutron behaviour in heterogeneous systems (Stacey, 2007). Even though the MSFR is closer to a homogeneous reactor than traditional solid-fuelled reactors, heterogeneities still exist at the blanket and reflector interfaces, or due to the presence of non-homogeneous bubble distributions in the fuel mixture. Therefore, a transport solver may be beneficial to the analysis of the MSFR helium bubbling system, especially when non-uniform bubble distributions are involved. In any case, a comparison to more accurate neutronics models can also be useful to assess the predictive capabilities and the conservativeness of neutron diffusion approaches, currently employed in the analysis of the MSFR, providing useful guidelines for future simulations. Due to the lack of specific literature on the subject, this is particularly important for the analysis of the helium bubbling system. The comparison of different modelling approaches, characterized by different levels of detail, is fundamental not only for the system design (as well as for the assessment of its safety and feasibility) but also to verify the suitability of the available simulation tools to handle this complex problem.

In this context, the two-phase solver presented in Cervi et al. (2017, 2018) is extended, implementing a neutronics module based on the SP_3 approximation of the neutron transport equation. Compared to available literature, this work presents the only CFD solver coupling neutron transport, compressible and two-phase thermal-hydraulics within the same simulation environment.

The paper is organized as follows. In Section 2, a brief description of the MSFR and of the helium bubbling system is provided. In Section 3, the general structure of the solver is described and the new SP_3 module is presented. In Section 4, the solver is tested against a Monte

Carlo model of the MSFR, assuming static and isothermal fuel (modelling assumptions that are traditionally adopted in standard Monte Carlo simulations) in order to assess its correct implementation. In Section 5, the multiphysics coupling between neutron transport and two-phase thermal-hydraulics is tested on a 2D axial-symmetric model of the MSFR, evaluating the void reactivity coefficients on the basis of the bubble spatial distribution calculated by the multiphysics solver. Conclusions and future research perspectives are provided in Section 6.

2. Investigated reactor concept

2.1. Description of the Molten Salt Fast Reactor

In this Section, the MSFR is briefly described in order to highlight some peculiarities of interest for the present work. A schematic representation of the MSFR layout is shown in Fig. 1, while the main design parameters used in this work are listed in Table 1. The salt mixture, which serves simultaneously as fuel and coolant, is circulated through sixteen external circuits, where the power produced by fissions is removed by heat exchangers. The flow direction of the fuel mixture is indicated in Fig. 1. The helium bubbles are injected in the cold legs, at the bottom of the system, and they are removed at the top, in the hot leg region.

3. The modelling approach

In this Section, the structure of the multiphysics solver adopted in this work is described. At each time step, the system thermal-hydraulics and neutronics are solved in two different cycles, as indicated in Fig. 2. The thermal-hydraulics sub-solver is based on the standard OpenFOAM solver "*twoPhaseEulerFoam*" for the compressible fluid and the bubble modelling. As for neutronics, a multi-group neutron diffusion sub-solver was developed in previous works (Cervi et al., 2017; 2018).

At the beginning of the time step, the thermal-hydraulics cycle solves for the phase fractions, for the velocity of both phases, for the pressure and for the temperature. Picard iterations are performed until convergence is reached for the solution of the thermal-hydraulic part of the problem. Then, the neutronics cycle begins, solving for the flux, for the delayed neutron precursors and for the decay heat. Once the flux (and the fission power in turn) and the decay heat are known, the volumetric power source field is updated and the energy equation is solved again. Once the new temperature and density fields of the fuel are calculated, the cross sections are updated and the cycle is repeated with Picard iterations until convergence is reached. In addition, a certain number of external iterations between the thermal-hydraulics and the neutronics sub-solvers is performed. The external iterations are particularly important in fast transients, in which the large thermal expansions due to steep power excursions have a strong impact on the fuel velocity field.

In the following sub-section, the new module based on the multi-group SP_3 transport equations is presented. More details on the thermal-hydraulics and neutron diffusion modules can be found in Cervi et al. (2017, 2019).

3.1. The SP_3 neutron transport module

In the spherical harmonics (or P_N) approximation, the angular dependence of the neutron flux is expanded into the first N spherical harmonics (Bell and Glasstone, 1970). The spherical harmonics expansion results in a complex system of $(N + 1)^2$ differential equations,

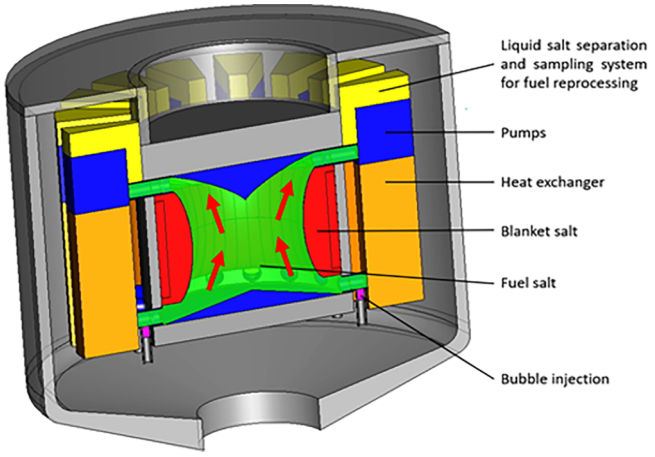

Fig. 1. Layout of the MSFR.

due to the dependence on both the components μ and φ of the angular variable Ω (Duerigen, 2013) and to complicate cross-derivative terms (Gerbard, 1968). For this reason, a simplified version of the P_N approximation – the so called SP_N equations – was proposed to overcome the model complexity while improving the accuracy with respect to the diffusion approach. The SP_N equations were first derived by (Gelbard, 1962), replacing the 1D second order derivative in a planar formulation of the P_N approximation with the 3D Laplacian operator, obtaining a system of $(N + 1)/2$ equations (Fiorina et al., 2017). Therefore, in the specific case of the SP_3 approximation, two equations must be solved for the first two even-order flux momenta, φ_0 and φ_2. Thanks to their simplicity and to their theoretically sound derivation (Brandtley and Larsen, 2000), the SP_3 equations can be regarded as compromise between accuracy and computational cost. Being obtained from a planar formulation of the P_3 approximation, the SP_3 equations are particularly suitable for systems in which the flux variation near interfaces is mainly one directional, which is often the case for nuclear reactors (Fiorina et al., 2017). This is expected to be even more true for the specific case of the MSFR, which compared to traditional reactors is closer to a homogeneous system. Details on the derivation of the SP_3 equations with full anisotropic scattering terms can be found in (Duerigen, 2013). A further simplification can be obtained by neglecting anisotropic scattering within different energy groups (Duerigen, 2013; Fiorina et al., 2017), i.e., assuming that:

$$\Sigma_{sn,gg'} = 0 \quad \text{for } g \neq g' \quad \text{and} \quad n \geq 1 \tag{1}$$

With this assumption, the SP_3 equations are merely coupled by the isotropic scattering terms, leading to a set of diffusion-like equations, known as *SP_3 within-group form*. Introducing the variable:

$$\Phi_{0,i} = \varphi_{0,i} + 2\varphi_{2,i} \tag{2}$$

the SP_3 equations can be finally written as follows:

$$\frac{1}{v_i}\frac{\partial \Phi_{0,i}}{\partial t} = \nabla \cdot D_{0,i} \nabla \Phi_{0,i} - \Sigma_{r,i}(\Phi_{0,i} - 2\varphi_{2,i}) + S_{n,i}(1-\beta)\chi_{p,i} + S_d \chi_{d,i} + S_{s,i} + \frac{2}{v_i}\frac{\partial \varphi_{2,i}}{\partial t} \tag{3}$$

$$\frac{9}{5}\frac{1}{v_i}\frac{\partial \varphi_{2,i}}{\partial t} = \nabla \cdot D_{2,i} \nabla \varphi_{2,i} - \Sigma_{t2,i}\varphi_{2,i} + \frac{2}{5}\Sigma_{r,i}(\Phi_{0,i} - 2\varphi_{2,i}) - \frac{2}{5}S_{n,i}(1-\beta)\chi_{p,i} - \frac{2}{5}S_d\chi_{d,i} - \frac{2}{5}S_{s,i} + \frac{2}{5}\frac{1}{v_i}\frac{\partial \Phi_{0,i}}{\partial t} \tag{4}$$

Table 1
Main design parameters of the MSFR (Gerardin et al., 2017; Tano et al., 2017).

Parameter	Value
Nominal power	3000 MW_{th}
Fuel inlet temperature	923 K
Fuel outlet temperature	1023 K
Total salt volume	18 m^3
Fuel composition (% mol.)	LiF (77.5) - ThF_4 (20.0) - $^{233}UF_4$ (2.5)

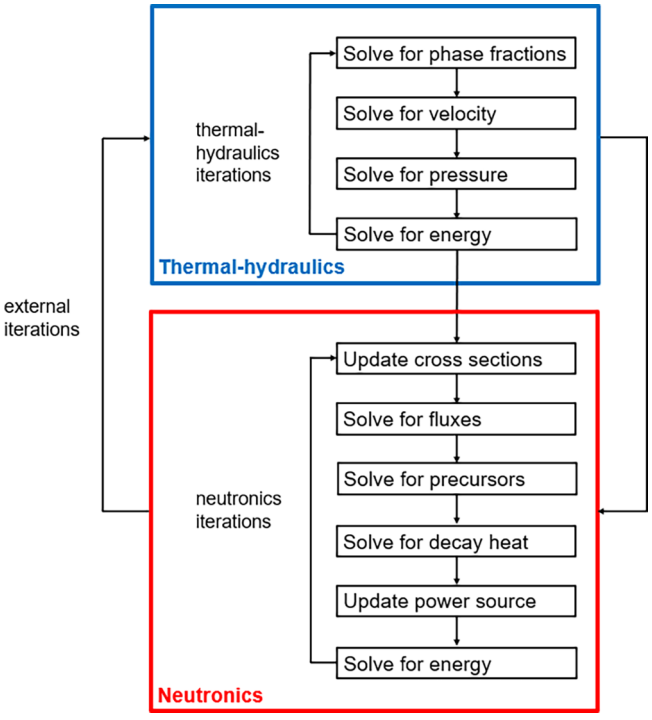

Fig. 2. Structure of the multiphysics solver.

where:

$$D_{0,i} = \frac{1}{\Sigma_{tr,i}} \tag{5}$$

$$\Sigma_{t2,i} = \Sigma_{t,i} - \Sigma_{s2,ii} \tag{6}$$

$$D_{2,i} = \frac{9}{35}\frac{1}{\Sigma_{t,i} - \Sigma_{s3,ii}} \tag{7}$$

The macroscopic cross sections are evaluated by assuming a logarithmic dependence on temperature and a linear dependence on density and on the void fraction, according to the following relation:

$$\Sigma_{i,j} = \left[\Sigma^{o}_{i,j} + A_{i,j} log\frac{T_{fuel}}{T_{ref}}\right]\frac{\rho_{fuel}}{\rho_{ref,fuel}}(1 - \alpha_b) \tag{8}$$

The source terms represent the fission neutrons, the scattering neutrons and the delayed neutrons, respectively, and are evaluated as follows:

$$S_{n,i} = \sum_j \bar{\nu}\Sigma_{f,j}\varphi_{0,j} \tag{9}$$

$$S_{s,i} = \sum_{j\neq i} \Sigma_{s,j\rightarrow i}\varphi_{0,j} \tag{10}$$

$$S_d = \sum_k \lambda_k c_k \tag{11}$$

Due to these explicit terms, an iterative procedure among the several groups is required to achieve convergence for the neutronics description. Albedo boundary conditions are adopted at the top and bottom walls of the reactor (axial reflectors) and at the radial wall (blanket salt), in order to limit the solution of the neutron diffusion equation to the fuel salt circuit only (Aufiero et al., 2014b; Fiorina et al., 2017). For the SP_3 equations, the albedo boundary conditions can be expressed, starting from the outgoing and the incoming neutron currents, as follows:

$$D_{0,i}\nabla\Phi_{0,i} = -\frac{1}{2}\left(\frac{1-\alpha_i}{1+\alpha_i}\right)\left(\Phi_{0,i} - \frac{3}{4}\varphi_{2,i}\right) \tag{12}$$

$$D_{2,i}\nabla\varphi_{2,i} = \frac{1}{2}\left(\frac{1-\alpha_i}{1+\alpha_i}\right)\left(\frac{3}{20}\Phi_{0,i} - \frac{21}{20}\varphi_{2,i}\right) \tag{13}$$

where the albedo coefficients α_i are the ratios between the outgoing and the incoming neutron currents.

The precursor balance equations include the diffusion and the transport term to allow for the fuel motion (neglecting the precursor mass transfer from the liquid to the gas phase):

$$\frac{\partial\rho_l\alpha_l c_k}{\partial t} + \nabla\cdot(\rho_l\alpha_l\boldsymbol{u}_l c_k) = \nabla\cdot\left(\rho_l\alpha_l\left(\frac{\nu}{Sc} + \frac{\nu_T}{Sc_T}\right)\nabla c_k\right) + \beta_k\sum_i \bar{\nu}\Sigma_{f,i}\varphi_i - \lambda_k\rho_l\alpha_l c_k \tag{14}$$

The turbulent Schmidt number Sc_T is set to 0.85, even if no data are specifically available for the diffusion of species in the MSFR salt (Aufiero et al., 2014b).

In order to properly consider the decay heat during accidental transients, the solver is provided with equations that consider the behaviour of the isotopes responsible for the decay heat, subdivided in "decay heat groups" in a manner similar to the precursor groups. Actually, the equations implement the balance for the precursor concentration multiplied by the average energy released by that decay group:

$$\frac{\partial\rho_l\alpha_l d_m}{\partial t} + \nabla\cdot(\rho_l\alpha_l\boldsymbol{u}_l d_m) = \nabla\cdot\left(\rho_l\alpha_l\left(\frac{\nu}{Sc} + \frac{\nu_t}{Sc_t}\right)\nabla d_m\right) + \beta_{h,l}\sum_i E_f\Sigma_{f,i}\varphi_i - \lambda_{h,l}\rho_l\alpha_l d_m \tag{15}$$

In addition, a power iteration routine, based on the k-eigenvalue method, is implemented in the neutronics module of the solver for the calculation of the multiplication factor. For a more detailed description, the reader is referred to (Cervi et al., 2017).

4. Comparison to Monte Carlo simulation

In this Section, the SP_3 and the previously implemented diffusion solvers are compared to the results of a Monte Carlo simulation carried out with the reactor physics code Serpent 2 (Leppänen et al., 2015). The purpose of the comparison is (i) to verify the correct implementation of both the neutronics modules and (ii) to assess the improvement in the predictive capabilities of the SP_3 approach over the diffusion one, with specific application to the analysis of the MSFR. To this aim, a simplified cylindrical geometry of the MSFR is adopted (Brovchenko et al., 2013). In the Serpent model, this geometry is reproduced in three dimensions, also including the solid regions of the reflectors, fertile blanket and boron carbide shield (see Fig. 3).

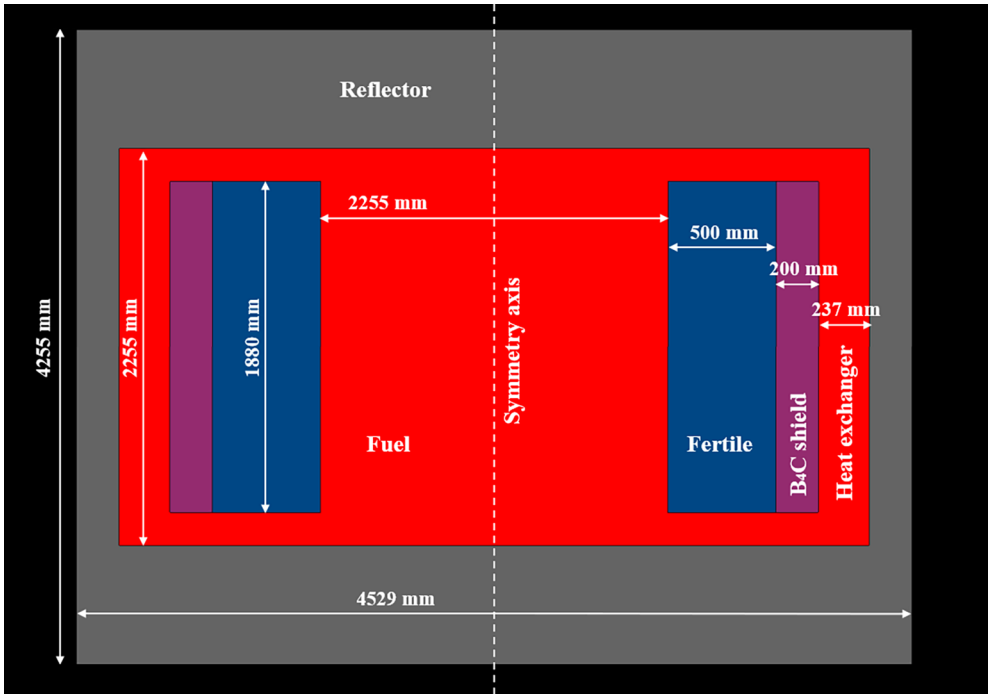

Fig. 3. Serpent simplified model of the MSFR.

Conversely, in the OpenFOAM model a 2D axial symmetric geometry is adopted (i.e., a slice of the cylinder, see Fig. 4), solving the equations in cylindrical coordinates. In addition, only the liquid part of the reactor is simulated, taking in account the fertile blanket and the reflectors by means of the albedo boundary conditions expressed by Eqs. (12) and (13).

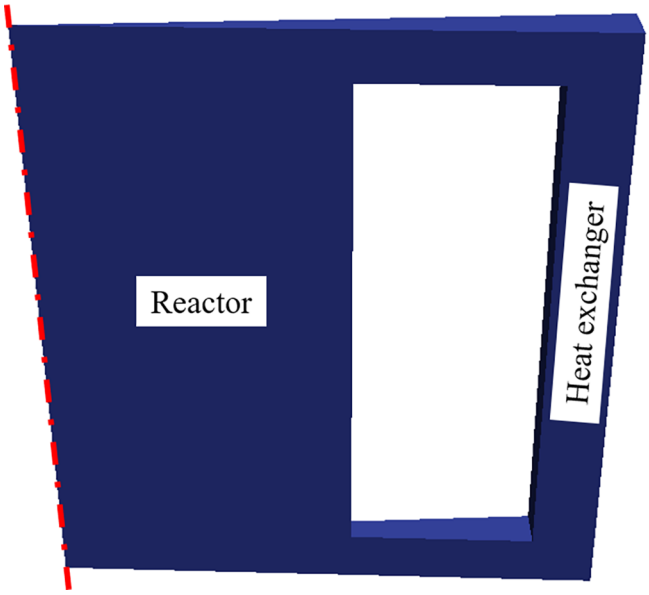

Fig. 4. OpenFOAM simplified model of the MSFR.

The purpose of this comparison is to assess the correct implementation and the predictive capabilities of the diffusion and transport modules implemented in the OpenFOAM solver. However, Monte Carlo and deterministic methods are two completely different approaches to study reactor physics, each of them having different advantages and drawbacks, as discussed below. Such differences may complicate a direct comparison between the two approaches, especially when complex multiphysics systems - such as the MSFR - are involved. For this reason, particular care is required to carry out all the simulations - the deterministic and the Monte Carlo ones - under conditions and modelling choices that make a comparison possible.

Typically, Monte Carlo simulations are carried out using a uniform temperature and density for each material. In addition, standard Monte Carlo codes cannot handle the precursor motion due to the circulating fuel, since they were originally developed for solid-fuel reactors.

On the other hand, the OpenFOAM multiphysics solver calculates space varying temperature and density fields and implements transport equations for the moving precursors. In addition, the present solver also has the capability to handle the presence of bubbles inside the reactor, calculating their spatial distribution (which is, in general, non-uniform). As mentioned above, these effects are not considered in Monte Carlo simulation, possibly hindering a direct and significant comparison between the two approaches. To overcome this issue, static fuel is also assumed in the OpenFOAM model, together with the adoption of a uniform temperature and density.

All the Monte Carlo calculations are carried out using 1.8 billion neutron histories (15000 generations of 120,000 particles), obtaining a 1 pcm 1-σ uncertainty on the multiplication factor. The convergence of the fission source has been granted analysing the Shannon entropy and adopting 1000 inactive cycles. The JEFF-3.1.1 (Santamarina et al., 2009) cross section library is selected for the Monte Carlo simulations. On the other hand, the OpenFOAM calculations are carried out adopting six energy groups, using homogenized cross sections generated by the Serpent model. The relative uncertainty of the generated multi-group cross sections is in the order of 10^{-2}%. Six-group albedo coefficients are also evaluated with Serpent by means of surface current detectors, placed at the liquid region boundary. The coefficient values depend on each specific material interface.

The energy group subdivision adopted in this work is shown in Table 2. This energy structure has been tested in previous works (Fiorina, 2013; Fiorina et al., 2013) against ERANOS (using 33 and 1968 energy groups) and Serpent, showing that it is capable to reproduce the overall shape of the neutron spectrum, and obtaining a good agreement in the prediction of different neutronics parameters. Two sets of cross sections are generated for T_{fuel} equal to 900 K and

1200 K, assuming a uniform fuel density of 4125 kg/m^3. Recalling Eq. (8), the cross section dependence on fuel temperature, fuel density and void fraction is expressed as follows:

$$\Sigma_{i,j}=\left[\Sigma^{o}_{i,j} + A_{i,j} log\frac{T_{fuel}}{T_{ref}}\right]\frac{\rho_{fuel}}{\rho_{ref,fuel}}(1-\alpha_b) \quad (8)$$

where the term $\Sigma^{o}_{i,j}$ corresponds to cross section value at 900 K, while $A_{i,j}$ is evaluated by interpolating the cross sections between 900 and 1200 K.

Table 2
Energy group division adopted in the present work.

Energy group	Energy ranges (MeV)
1	2.23 ÷ 20.00
2	$4.98{\cdot}10^{-1}$ ÷ 2.23
3	$2.48{\cdot}10^{-2}$ ÷ $4.98{\cdot}10^{-1}$
4	$5.53{\cdot}10^{-3}$ ÷ $2.48{\cdot}10^{-2}$
5	$7.49{\cdot}10^{-4}$ ÷ $5.53{\cdot}10^{-3}$
6	0 ÷ $7.49{\cdot}10^{-4}$

Firstly, the multiplication factor is evaluated by means of the Serpent and of the OpenFOAM solver, using both the SP_3 and the diffusion modules. Results for different temperatures and void fractions are compared in Table 3.

Table 3
Multiplication factor from the Monte Carlo, SP_3 and diffusive neutronics models.

T_{fuel}(K)	$\bar{\alpha_b}$(%)	$k_{SERPENT}$ ± 2-σ uncertainty	k_{SP3} (difference with respect to Serpent in pcm)	$k_{diffusion}$ (difference with respect to Serpent in pcm)
900	0	0.991320 ± 0.000020	0.985082 (−623.8)	0.983806 (−751.4)
900	1	0.989860 ± 0.000020	0.983585 (−626.7)	0.982269 (−759.1)
900	2	0.988310 ± 0.000020	0.982048 (−626.2)	0.980691 (−761.9)
900	3	0.986780 ± 0.000020	0.980474 (−630.6)	0.979075 (−770.5)
1000	0	0.987400 ± 0.000020	0.981158 (−624.2)	0.979892 (−750.8)
1100	0	0.983900 ± 0.000020	0.977676 (−622.4)	0.976419 (−748.1)
1200	0	0.980720 ± 0.000020	0.974551 (−616.9)	0.973302 (−741.8)

In addition, the Doppler constant is calculated as:

$$K_D = \frac{\rho(T_{fuel,2}) - \rho(T_{fuel,1})}{log\left(\frac{T_{fuel,2}}{T_{fuel,1}}\right)} \quad (16)$$

The values of the Doppler constants calculated at different fuel temperature ranges using Serpent, the transport and the diffusion solvers are listed in Table 4. The aim of this comparison is to evaluate the agreement between the OpenFOAM and the Monte Carlo results not only at the interpolation temperatures (i.e., 900 K and 1200 K), but also at intermediate values.

Then, the void reactivity coefficient is evaluated using the following relation:

$$\alpha_{void} = \frac{\rho(\bar{\alpha_b}) - \rho(0)}{\bar{\alpha_b}} \quad (17)$$

where $\bar{\alpha_b}$ is the core-average percent void fraction, assumed, for the present calculation, equal to 1%. As explained above, a uniform void fraction is assumed in this comparison. A comparison of the void coefficients obtained with Serpent, the transport and the diffusion models can be found in Table 5. Note that a uniform variation of the void fraction is equivalent to a uniform density effect. Therefore, the void coefficients can be easily expressed in terms of pcm per unit density, and the results of Table 5 are also representative as a comparison of the density reactivity coefficients.

Table 5
Void reactivity coefficient from the Monte Carlo, SP_3 and diffusive neutronics models.

$\bar{\alpha_b}$(%)	$\alpha_{void,SERPENT}$ ± 2-σ uncertainty (pcm/%)	$\alpha_{void,SP3}$(pcm/%) (% relative difference with respect to Serpent)	$\alpha_{void,diffusion}$(pcm/%) (% relative difference with respect to Serpent)
1	−148.8 ± 4.0	−154.7 (−4.0)	−159.1 (−6.9)
2	−153.6 ± 2.0	−156.8 (−2.1)	−161.4 (−5.1)
3	−154.7 ± 1.4	−159.0 (−2.8)	−163.7 (−5.8)

Finally, a comparison of the axial and radial total flux profiles at reactor mid-planes is presented in Figs. 5 and 6, respectively, while the peak values of the flux are compared in Table 6. In all the simulations, the total fission power is normalized to 3000 MW to evaluate the flux profiles.

4.1. Discussion of results

The SP_3 solver shows a better agreement with Monte Carlo simulation, compared to the diffusion module, in the prediction of the multiplication factor (Table 3). In particular, the error with respect to the Serpent model is reduced from ~750–770 pcm with the diffusion solver to ~620–630 pcm with the SP_3 solver.

As for the Doppler constant, the outcomes of the SP_3 and of the diffusion solvers are coincident up to the first decimal digit and are in excellent agreement with Monte Carlo results in all the investigated temperature ranges (Table 4). Finally, with the SP_3 solver, the error in the void reactivity coefficient is reduced from ~5–7% to ~2–4% (Table 5).

General better agreement is also shown by the SP_3 total flux profiles (Figs. 5 and 6), especially in the centre of the reactor, where the peak value of the total flux is predicted with a smaller error (6% vs. 7%) – see Table 6. This discrepancy is a normalization effect, due to the fact that the same total fission power (i.e., 3000 MW) is imposed in all the calculations.

Table 4
Doppler coefficient from the Monte Carlo, SP_3 and diffusive neutronics models.

T_{fuel} (K)	$K_{D,SERPENT}$ ± 2-σ uncertainty (pcm)	$K_{D,SP3}$(pcm) (difference with respect to Serpent in pcm)	$K_{D,diffusion}$(pcm) (difference with respect to Serpent in pcm)
900 ÷ 1000 K	−3801.0 ± 38.8	−3853.4 (−52.4)	−3853.4 (−52.4)
1000 ÷ 1100 K	−3779.9 ± 43.2	−3808.5 (−28.9)	−3808.5 (−28.4)
1100 ÷ 1200 K	−3787.5 ± 47.6	−3769.4 (−18.1)	−3769.4 (−18.1)

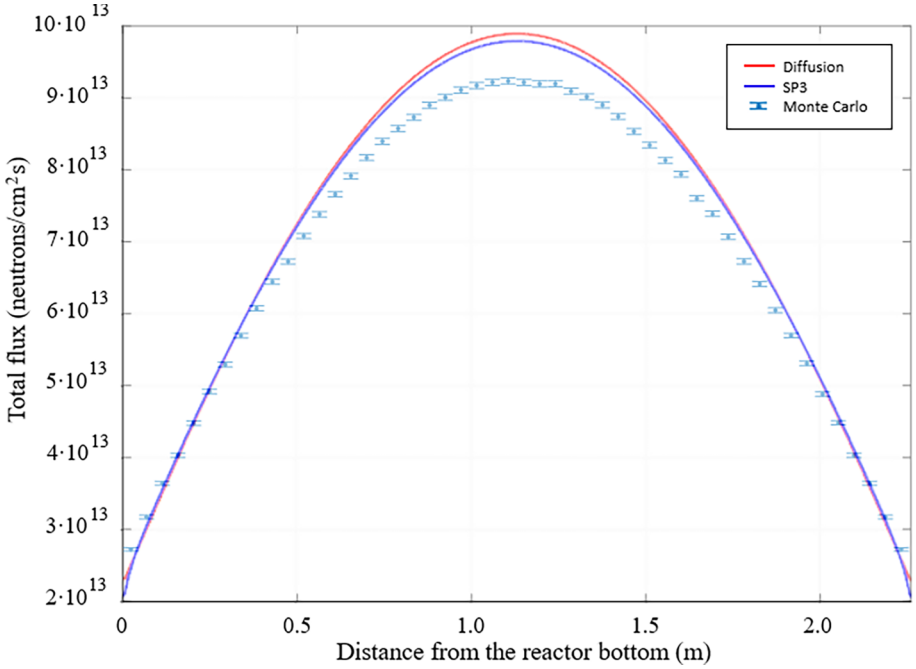

Fig. 5. Total flux axial profiles (along the reactor symmetry axis) from Monte Carlo (with 2-σ uncertainty bars), SP3 and diffusive neutronics models.

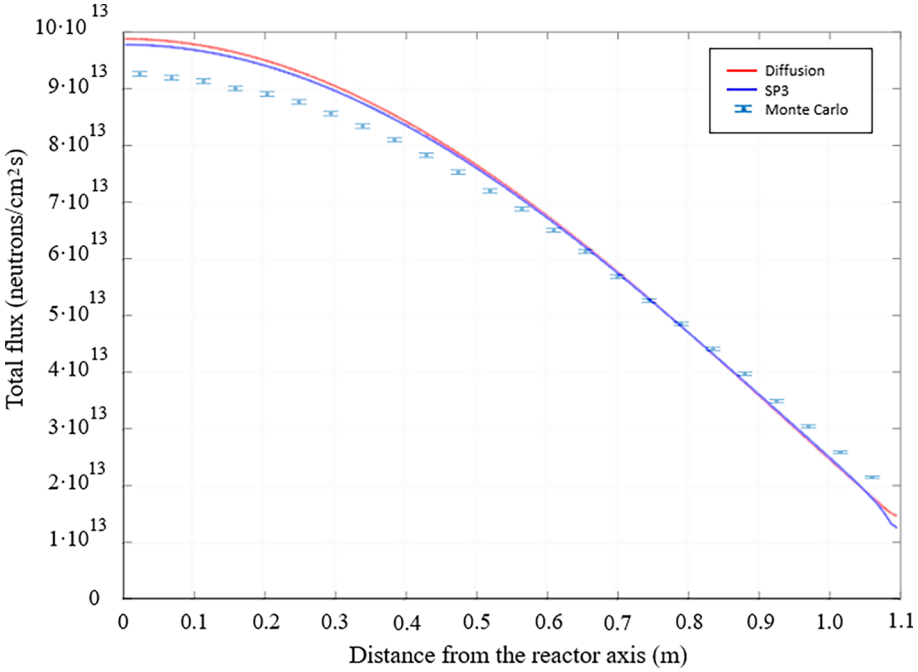

Fig. 6. Total flux radial profiles (at reactor half-height) from the Monte Carlo (with 2-σ uncertainty bars), SP_3 and diffusive neutronics models.

Table 6
Peak total fluxes from the Monte Carlo, SP_3 and diffusive neutronics models.

Serpent peak flux ± 2-σ uncertainty (neutrons/cm^{2}s)	SP_3 peak flux (neutrons/cm^{2}s) (% relative difference with respect to Serpent)	Diff. peak flux (neutrons/cm^{2}s) (% relative difference with respect to Serpent)
$(9.24 \pm 0.04)\cdot10^{13}$	$9.79\cdot10^{13}$ (6.0)	$9.89\cdot10^{13}$ (7.0)

In general, both the SP_3 and the diffusion results are in good agreement with the Monte Carlo solution, suggesting that both those modules are correctly implemented. The 600–700 pcm errors in the multiplication factor calculations are mainly due to the adoption of a different geometry between the Monte Carlo and the OpenFOAM model, being the latter without the blanket and the reflectors zones. This lack is partially balanced with the albedo boundary conditions, that are relevant in order to reduce the complexity of the coupled

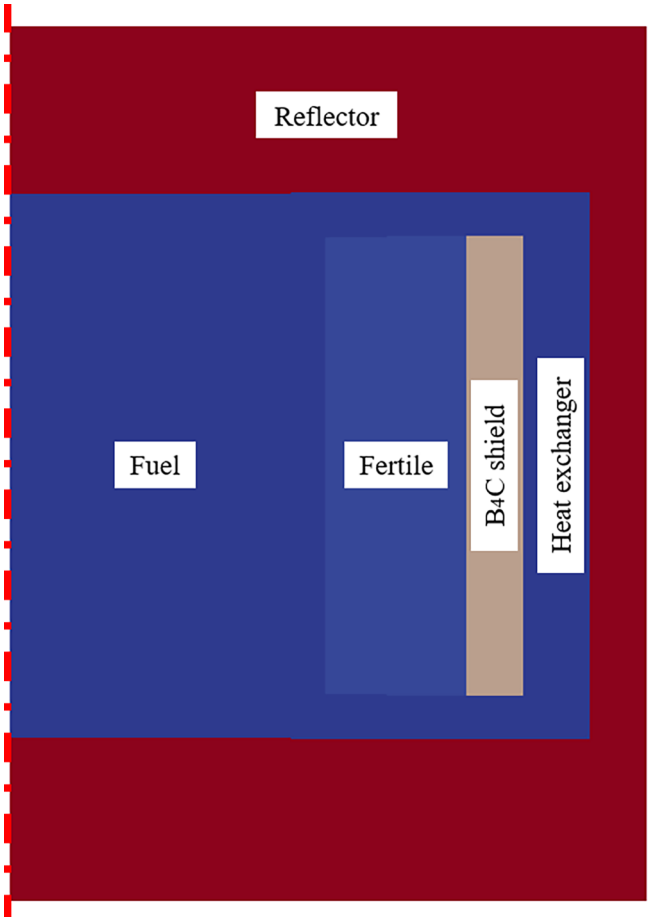

Fig. 7. OpenFOAM simplified model of the MSFR including the solid blanket and reflectors.

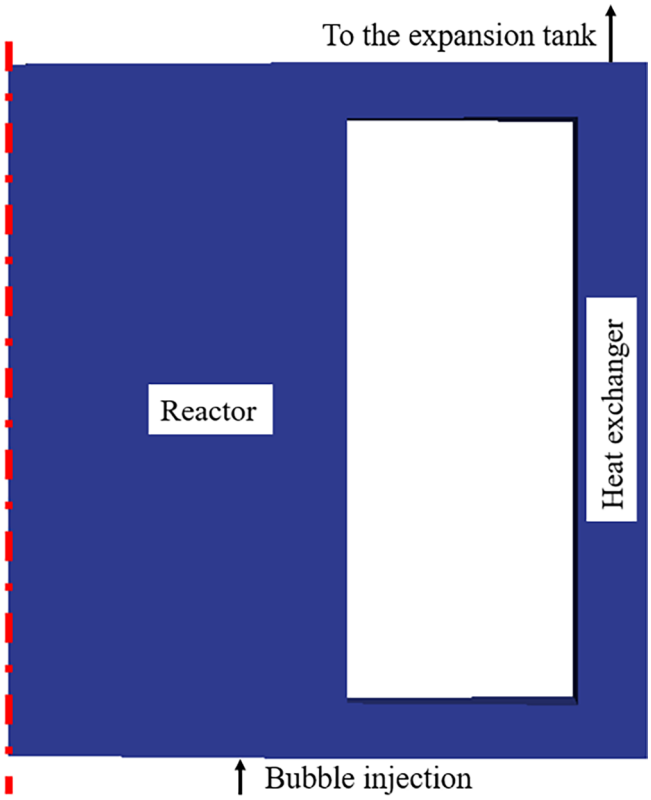

Fig. 8. OpenFOAM model of the MSFR with the helium bubbling system.

neutronics and thermal-hydraulics simulations. In this regard, it is worth mentioning that the purpose of the present work is not the accurate estimation of absolute reactivity, but rather the evaluation of reactivity variations (i.e., the reactivity coefficients) which are well predicted using albedo boundary conditions. In particular, the aim of this work is the correct evaluation of the void reactivity coefficient, which is of interest for the analysis of the helium bubbling system. Therefore, the k_{eff} errors obtained with the albedo boundary conditions are acceptable for the purposes of this study. In addition, these errors are consistent with other works carried out with the same approach (Aufiero et al., 2014b). In order to prove the main source of discrepancy in the multiplication factor estimation between the Monte Carlo and OpenFoam model, a simplified version of the latter has been developed, including the reflectors and the blanket in the OpenFOAM model (Fig. 7). In this case, the errors are reduced to about -230 pcm with the SP_3 module and to about -260 pcm with the diffusion module (Table 7).

In general, the transport correction improves the estimation of the multiplication factor, of the void coefficient and of the neutron flux as well, reducing the errors with respect to Monte Carlo simulations. The reduction of the void coefficient errors is of particular interest for the analysis of the helium bubbling system, which is carried out in Section 5. Conversely, the SP_3 and the diffusion modules predict the same values of the Doppler constants, both being in good agreement with Monte Carlo simulation.

5. Analysis of the MSFR helium bubbling system

The purpose of this Section is the analysis of the MSFR helium bubbling system and its effect on reactivity, highlighting the differences between the results of the transport and the diffusion solvers. As opposed to Section 4, where isothermal and static fuel was assumed, the temperature, density and velocity fields of the fuel are evaluated by the multiphysics solver, according to the coupling scheme described in Fig. 2. The helium bubbles are injected at the bottom of the reactor and are extracted at the top, before the heat exchanger region (see Fig. 8). A complete description of the adopted thermal-hydraulics model can be found in Cervi et al. (2019). In particular, the injection and extraction systems have been modelled as a mass source and sink, respectively,

Table 7
Multiplication factor from the Monte Carlo, SP_3 and diffusive neutronics models (for $T_{fuel} = 900K$ and $\bar{\alpha}_b = 0$).

$k_{SERPENT}$ ± 2-σ uncertainty	k_{SP3} (difference with respect to Serpent in pcm)	$k_{diffusion}$ (difference with respect to Serpent in pcm)
0.991320 ± 0.000020	0.989035 (−228.5)	0.988753 (−256.7)

since no detailed information is currently available on the design of these systems. No-slip boundary conditions are imposed for the fuel and gas velocity at the reactor walls, while atmospheric pressure is imposed at the expansion tank. The Lahey k-ε turbulence model (Lahey, 2005) has been adopted to account for the contribution of the dispersed gaseous phase on eddy viscosity.

In this section, the void reactivity coefficient is evaluated on the basis of the bubble spatial distribution calculated by the multiphysics solver, pointing out differences with respect to the calculation performed by means of uniform void fraction distributions.

The presence of bubbles in the reactor introduces a negative reactivity into the system, due to the negative void reactivity coefficient. For this reason, the helium bubbling system is foreseen as a possible option for the reactivity control of the MSFR. In any case, should other options be preferred, the helium bubbling system would still be employed for the removal of gaseous fission products. Therefore, careful investigation is required to assess the safety and the feasibility of this design choice, as well as its effect on the system reactivity.

A preliminary evaluation of the bubbly flow contribution to the system reactivity can be made by assuming a uniform bubble distribution. This could be achieved by Monte Carlo simulation or with a standard single-phase thermal-hydraulic model, simply correcting the fuel density by a uniform void fraction. On the other hand, the real distribution of the bubbly flow inside the reactor is not uniform, since the bubble are transported by the fuel mixture. For this reason, the void coefficient needs to be evaluated accounting for the spatial and neutron importance dependence of the bubble reactivity effect. The multiphysics solver, thanks to the coupling between neutronics and two-phase thermal-hydraulics, has the capability to deal with this aspect of the void reactivity effect. To highlight this effect, the void coefficient is evaluated with two different approaches:

- Case 1: the bubble spatial distribution calculated by the multiphysics solver is considered.
- Case 2: a uniform bubble distribution is assumed, with the same core-average value of Case 1.

In both cases, the void coefficient is calculated using Eq. (17). The multiplication factor and the void reactivity coefficient evaluated at different void fractions with the diffusion and the SP_3 modules are listed in Tables 8 and 9, respectively. Fig. 9 shows the void fraction distributions (i.e., the volume fraction occupied by the helium) and the power density distributions evaluated by means of the SP3 module for $\bar{\alpha}_b$ equal to 0.635% and 1.468% (these are the steady-state average void fractions for two different helium injection flow rates, 0.1 and 0.2 g/s, respectively).

Table 8
Multiplication factor and void faction evaluated with the diffusion solver.

Core-average void fraction (%)	Multiplication factor		Void coefficient (pcm/%)	
	Case 1 (calculated bubble distribution)	*Case 2 (uniform bubble distribution)*	*Case 1 (calculated bubble distribution)*	*Case 2 (uniform bubble distribution)*
0	0.976288	0.976288	–	–
0.288	0.975304	0.975844	−358.8	−161.8
0.635	0.974301	0.975304	−329.0	−162.7
1.030	0.973271	0.974684	−308.3	−163.7
1.468	0.972216	0.973990	−292.2	−164.6

Table 9
Multiplication factor and void faction evaluated with the SP_3 solver.

Core-average void fraction (%)	Multiplication factor		Void coefficient (pcm/%)	
	Case 1 (calculated bubble distribution)	*Case 2 (uniform bubble distribution)*	*Case 1 (calculated bubble distribution)*	*Case 2 (uniform bubble distribution)*
0	0.977592	0.977592	–	–
0.288	0.976652	0.977157	−341.9	−158.1
0.635	0.975674	0.976632	−316.7	−158.3
1.030	0.974669	0.976028	−297.8	−159.1
1.468	0.973642	0.975352	−282.7	−160.0

5.1. Discussion of results

Both with the diffusion and the SP_3 modules, a noticeable difference is observed between the void coefficients obtained in Case 1 (calculated bubble distribution) and in Case 2 (uniform bubble distribution). In particular, when a uniform distribution is assumed, the void reactivity coefficient has a value of about −160 pcm/%. This value is still comparable with the results of Section 4 for the static and isothermal fuel, even if some differences arise due to the different temperature and precursor distribution.

On the other hand, when the bubble distribution calculated by the multiphysics solver is considered, the void coefficient strongly increases (i.e., it becomes more negative), reaching values between −360 and −280 pcm/%. This outcome highlights a strong dependence of the void reactivity effect on spatial and neutron importance effects. In particular, in Case 1 (calculated bubble distribution), most of the bubbles are concentrated in the central region of the reactor, where the neutron importance is higher. For this reason, the void reactivity effect is stronger than in Case 2 (uniform bubble distribution), where a significant part of the bubbles is located in the peripheral regions of the reactor, where the neutron importance is lower. In addition, the presence of bubbles in the centre of the system shifts the power production towards the outer regions of the core. This can lead in turn to an increase of neutron leakages, possibly contributing to the higher void coefficient observed in Case 1 (calculated bubble distribution).

Moreover, when the calculated bubble distribution is considered (Case 1), it can be observed that the void coefficient decreases as the average void fraction increases. In fact, the bubbly flow decreases fissions in the centre of the reactor (see Fig. 8), reducing the neutron importance in this region. As a consequence, the marginal reactivity effect due to further helium addition decreases for higher void fractions.

As in Section 4, the diffusive neutronics model overestimates the void coefficient, compared to the SP_3 model, both in Cases 1 and 2. For comparison, the absolute and relative percent differences between the void coefficients obtained with the diffusion and the SP_3 modules are reported in Table 10 for Case 1 (calculated bubble distribution) and in Table 11 for Case 2 (uniform bubble distribution). Even if general good agreement is obtained, the error between the two approaches is not negligible. This is particularly true for Case 1, in which the non-uniformity of the bubble distribution increases the difference between the two methods. In fact, for the considered fuel composition, the effective delayed neutron fraction of the system is as low as 120–150 pcm (Aufiero et al., 2014a). Therefore, even ~10–20 pcm/% differences in the void reactivity coefficient - which are observed in Case 1 - can have

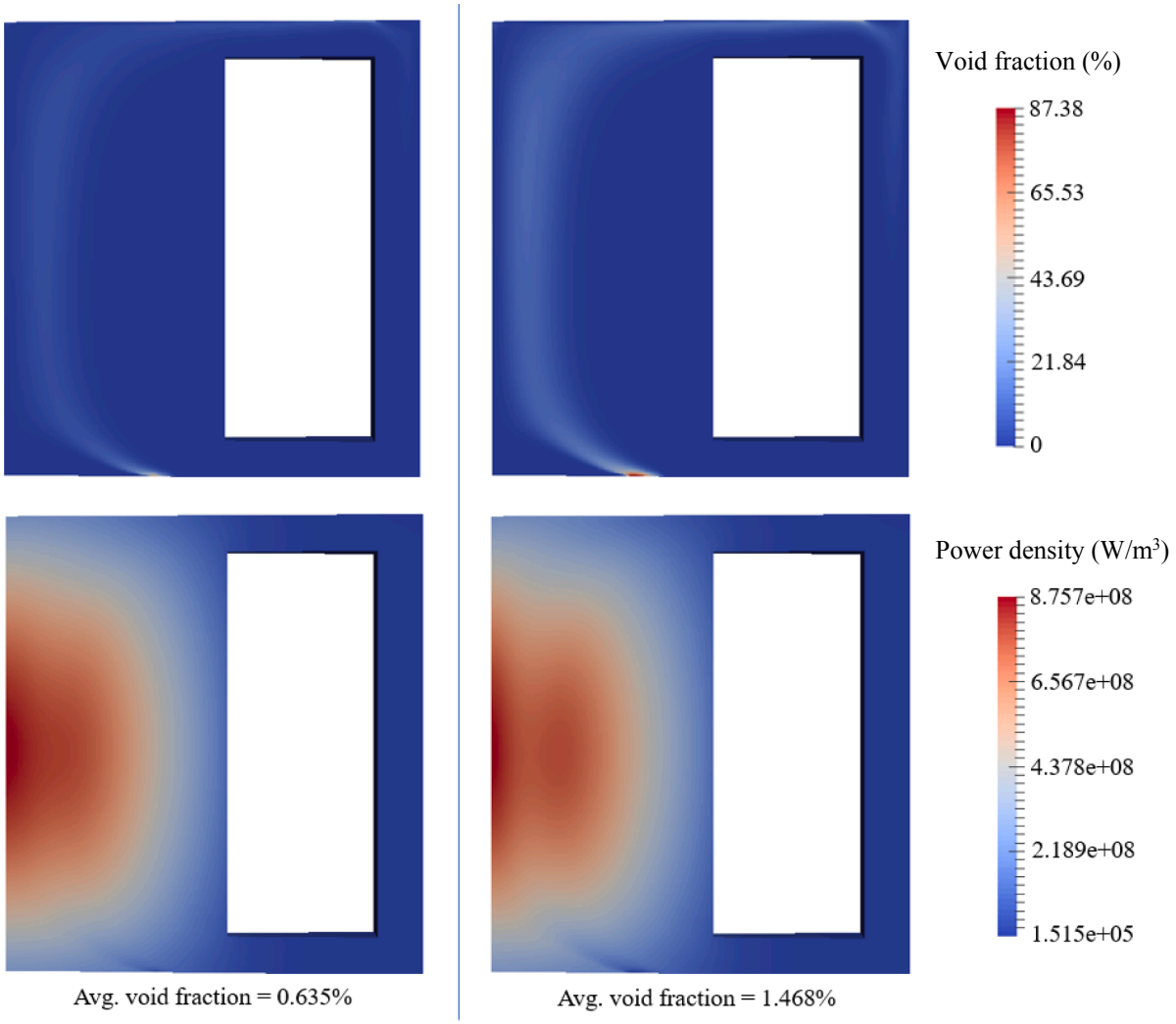

Fig. 9. Void fraction and power density distributions at 0.635% (left) and 1.468% (right) core average void fraction. The SP_3 module is used in these calculations.

Table 10
Absolute and relative difference between the void reactivity coefficient evaluated with the diffusion and SP_3 solvers in Case 1 (calculated bubble distribution).

Core-average void fraction (%)	Absolute difference (pcm/%)	Relative difference (%)
0.288	−16.9	−4.9
0.635	−12.3	−3.9
1.030	−10.5	−3.5
1.468	−9.5	−3.4

Table 11
Absolute and relative difference between the void reactivity coefficient evaluated with the diffusion and SP_3 solvers in Case 2 (uniform bubble distribution).

Core-average void fraction (%)	Absolute difference (pcm/%)	Relative difference (%)
0.288	−3.7	−2.3
0.635	−4.4	−2.8
1.030	−4.6	−2.9
1.468	−4.6	−2.9

a relevant impact on the system dynamics behaviour and, as a consequence, on the reactor operation and control.

Concerning computational requirements, the bottleneck in runtime is represented by the solution of the thermal-hydraulics part of the problem. Therefore, the addition of a further equation for the second flux moment (i.e., the adoption of the SP_3 approach) increases the computational time by only 17%. In view of this, and of the improved agreement with Monte Carlo simulations (see Section 4), the adoption of an SP_3 transport approximation model can constitute a valuable addition to the multiphysics analysis of the MSFR.

6. Conclusions and future development

An SP_3 neutron transport module is developed as an extension of a multiphysics OpenFOAM solver for the MSFR (Cervi et al., 2019), which couples a previously implemented diffusion module for neutronics and a two-fluids model for two-phase, compressible thermal-hydraulics. In this work, both the SP_3 and the diffusion modules are successfully verified against a Serpent model of the MSFR. The SP_3 solver yields sensible improvements in the prediction of the multiplication factor and of the void reactivity coefficient, even if both the modules show in general a good agreement with Monte Carlo results.

After testing, the multiphysics solver is applied to a 2D simplified model of the MSFR. The void reactivity coefficient is calculated on the basis of the bubble spatial distribution calculated by the multiphysics

solver. Important differences are highlighted with respect to simulations carried out with uniform bubble distributions. These results point out that the void reactivity effect is strongly dependent on spatial as well as on neutron importance effects. Significant differences are also highlighted between the diffusion and the SP_3 approaches, which can be relevant both for the optimization of the helium bubbling system as well as for the development of proper control strategies. The adoption of a more detailed neutronics model is particularly important when non-uniform bubble distributions are involved, which is the case of the MSFR.

Compared to available literature, the proposed solver is the only one coupling an SP_3 neutron transport approximation model with a two-phase, compressible thermal-hydraulics model. Therefore, this work constitutes a step forward in the multiphysics analysis of the MSFR, with a particular focus on the optimization of the helium bubbling system as well as on the development of reactivity control strategies.

Further benchmark and verification activities are ongoing, in order to assess the capabilities of the present solver to reproduce experimental data. Future efforts will be devoted to the extension of the multiphysics solver, including the modelling of the solid parts of the reactors (i.e., the top and bottom reflectors and the fertile blanket). In this regard, the development and the assessment of a thermal-mechanics module is currently ongoing (Cervi et al., 2018). The new module implements a dynamic mesh to describe the solid material deformations and is coupled to the neutronics modules to catch the thermal-mechanics feedback on reactivity. Wall deformation effects may be particularly important in the MSFR in case of fast, reactivity-driven transients, as highlighted by Cervi et al. (2019). More in general, a coupled neutronics and thermal-mechanics solver may be of interest for the analysis of other Generation IV systems, in which the thermal expansion of the fuel pins is expected to have important feedbacks on reactivity.

Acknowledgement

This project has received funding from the EURATOM research and training programme 2014-2018 under grant agreement No 661891.

Disclaimer

The content of this paper does not reflect the official opinion of the European Union. Responsibility for the information and/or views expressed therein lies entirely with the authors.

References

Aufiero, M., Cammi, A., Geoffroy, O., Losa, M., Luzzi, L., Ricotti, M.E., Rouch, H., 2014b. Development of an OpenFOAM model for the Molten Salt Fast Reactor transient analysis. Chem. Eng. Sci. 111, 78–90.

Aufiero, M., Brovchenko, M., Cammi, A., Clifford, I., Geoffroy, O., Heuer, D., Laureau, A., Losa, M., Luzzi, L., Merle, E., Ricotti, M.E., 2014a. Calculating the effective delayed neutron fraction in the Molten Salt Fast Reactor: analytical, deterministic and Monte Carlo approaches. Ann. Nucl. Energy 65, 390–401.

Bell, G.I., Glasstone, S., 1970. Nuclear Reactor Theory. Van Nostrand Reinhold Company, New York.

Brandtley, P.S., Larsen, E.W., 2000. The simplified P_3 approximation. Nucl. Sci. Eng. 134, 1–21.

Brovchenko, M., Merle, E., Rouch, H., Alcaro, F., Allibert, M., Aufiero, M., Cammi, A., Dulla, S., Feynberg, O., Frima, L., Geoffroy, O., Heuer, D., Ignatiev, V., Kloosterman, J.L., Lathouwers, D., Laureau, A., Luzzi, L., Merk, B., Ravetto, P., Rineiski, A., Rubiolo, P., Rui, L., Szieverth, M., Wang, S., Yamaji, B., 2013. Optimization of the preconceptual design of the MSFR, EVOL Evaluation and Viability of Liquid Fuel Fast Reactor System.

Cammi, A., Di Marcello, V., Luzzi, L., Memoli, V., Ricotti, M.E., 2011. A multi-physics modelling approach to the dynamics of Molten Salt Reactors. Ann. Nucl. Energy 38 (6), 1356–1372.

Cammi, A., Fiorina, C., Guerrieri, C., Luzzi, L., 2012. Dimensional effects in the modelling of MSR dynamics: moving on from simplified schemes of analysis to a multi-physics modelling approach. Nucl. Eng. Des. 246, 12–26.

Cervi, E., Lorenzi, S., Cammi, A., Luzzi, L., 2017. An Euler-Euler multi-physics solver for the analysis of the helium bubbling system in the MSFR. NENE 2017 26th International Conference Nuclear Energy for New Europe. Bled, Slovenia.

Cervi, E., Lorenzi, S., Luzzi, L., Cammi, A., 2018. An OpenFOAM solver for criticality safety assessment in dynamic compression events. ANS Winter Meeting & EXPO 2018. Orlando, USA.

Cervi, E., Lorenzi, S., Cammi, A., Luzzi, L., 2019. Development of a multiphysics model for the study of fuel compressibility effects in the Molten Salt Fast Reactor. Chem. Eng. Sci. 193, 379–393.

Delpech, S., Merle-Lucotte, E., Heuer, D., Allibert, M., Ghetta, V., Le-Brun, C., Mathieu, L., Picard, G., 2009. Reactor physics and reprocessing scheme for innovative molten salt reactor system. J. Fluor. Chem. 130 (1), 11–17.

Dolan, T.J., 2017. Molten Salt Reactors and Thorium Energy, Woodhead Publishing Series in Energy. Elsevier Ltd., Cambridge, MA, United States.

Duerigen, S., 2013. Neutron transport in hexagonal reactor cores modelled by trigonal-geometry diffusion and simplified P3 nodal methods, HZDR technical report.

Fiorina, C., Aufiero, M., Cammi, A., Franceschini, F., Krepel, J., Luzzi, L., Mikityuk, K., Ricotti, M.E., 2013. Investigation of the MSFR core physics and fuel cycle characteristics. Progr. Nucl. Energy 68, 153–158.

Fiorina, C., Lathouwers, D., Aufiero, M., Cammi, A., Guerrieri, C., Kloosterman, J.L., Luzzi, L., Ricotti, M.E., 2014. Modelling and analysis of the MSFR transient behaviour. Ann. Nucl. Energy 64, 485–498.

Fiorina, C., Hursin, M., Pautz, A., 2017. Extension of the GeN-Foam neutronic solver to SP_3 analysis and application to the CROCUS experimental reactor. Ann. Nucl. Energy 101, 419–428.

Fiorina, C., 2013. The molten salt fast reactor as a fast spectrum candidate for thorium implementation, (Ph.D. thesis).

Gelbard, E.M., 1962. Applications in the simplified spherical harmonics equations in spherical geometry. Technical Report WAPD-TM-294. Bettis Atomic Power Laboratory.

Gerardin, D., Allibert, M., Heuer, D., Laureau, A., Merle-Lucotte, E., Seuvre, C., 2017. Design evolutions of Molten Salt Fast Reactor. International Conference on Fast Reactors and Related Fuel Cycles: Next Generation Nuclear Systems for Sustainable Development (FR17). Yekaterinburg, Russia.

Gerbard, E.M., 1968. Spherical Harmonics Methods: P_L and Double-P_L Approximations. Gordon and Breach Science Publishers, New York, pp. 271–358.

Hu, T., Cao, L., Wu, H., Du, X., He, M., 2017. Coupled neutronics and thermal-hydraulics simulation of molten salt reactors based on OpenMC/TANSY. Ann. Nucl. Energy 109, 260–276.

Lahey, R.T., 2005. The simulation of multidimensional multiphase flows. Nucl. Eng. Des. 235, 1043–1060.

Leppänen, J., Pusa, M., Viitanen, T., Valtavirta, V., Kaltiaisenaho, T., 2015. The Serpent Monte Carlo code: status, development and application in 2013. Ann. Nucl. Energy 82, 142–150.

Moukalled, F., Mangani, L., Darwish, M., 2016. The Finite Volume Method in Computational Fluid Dynamics. Springer, New York.

OpenFOAM, 2013. OpenFOAM Documentation, available at < http://www.openfoam.org/docs/ > .

Ragusa, J.C., Mahadevan, V.S., 2009. Consistent and accurate schemes for coupled neutronics thermal-hydraulics reactor analysis. Nucl. Eng. Des. 239, 566–579.

Rusche, H., 2002. Computational Fluid Dynamics of Dispersed Two-Phase Flows at High Phase Fractions, (Ph.D. thesis).

Santamarina, A., Bernard, D., Blaise, P., Coste, M., Courcelle, A., Huynh, T.D., Jouanne, C., Leconte, P., Litaize, O., Ruggiéri, J-M., Sérot, O., Tommasi, J., Vaglio, C., Vidal, J-F., 2009. The JEFF-3.1.1 Nuclear Data Library, JEFF Report 22, OECD/NEA.

Serp, J., Allibert, M., Beneš, O., Delpech, S., Feynberg, O., Ghetta, V., Heuer, D., Holcomb, D., Ignatiev, V., Kloosterman, J.L., Luzzi, L., Merle, E., Uhlíř, J., Yoshioka, R., Zhimin, D., 2014. The molten salt reactor (MSR) in generation IV: overview and perspectives. Prog. Nucl. Energy 77, 308–319.

Stacey, W.M., 2007. Nuclear Reactor Physics. Wiley-VCH, Weinheim.

Tano, M., Rubiolo, P., Doche, O., 2017. Progress in modelling solidification in molten salt coolants. Model. Simul. Mater. Sci. Eng. 25, 1–29.

Wang, S., Rineiski, A., Maschek, W., 2006. Molten salt related extensions of the SIMMER-III code and its application for a burner reactor. Nucl. Eng. Des. 236, 1580–1588.